Original Research Article: full paper

(2023), «EUREKA: Physics and Engineering»
Number 1

DEVELOPMENT OF A HARDWARE EMULATOR OF A NANOSATELLITE GYROSCOPE

Aziz El Fatimi✉
Department of Electrical Engineering[1]
azizelfatimi@research.emi.ac.ma

Adnane Addaim
Department of Electrical Engineering[1]

Zouhair Guennoun
Department of Electrical Engineering[1]

[1]*Smart Communications Research Team (SCRT)*
University Center for Research in Space Technologies (CURTS)
Mohammadia School of Engineers (EMI)
Mohammed V University in Rabat (UM5R)
Ibn Sina ave., B.P 765, Agdal, Rabat, Morocco, 10090

✉**Corresponding author**

Abstract

The gyroscope sensor has multiple applications in consumer electronics, aircraft navigation, and control systems. Significant errors that match the corresponding data are a typical disadvantage of this sensor. This needs to be done by making error models that can be used to get the right level of measurement accuracy. For high-precision space applications, the navigation design system should take into account the angle random walk (N), bias instability error (B), and rate random walk (K) of the BMG160 gyroscope. For this reason, this paper shows how to use Allan Variance (AVAR) and Power Spectral Density (PSD) for the experimental identification and modeling of the stochastic parameters of the Bosch BMG160 gyroscope embedded in a nanosatellite in order to get an accurate gyroscope model. This work also demonstrates the principle of operation of the equivalent electronic model intended to carry out advanced simulations without recourse to the real material in order to avoid the problem of bad manipulation and availability of the material in order to reduce the time and cost of development. The interpretation of the Allan curves and the PSD obtained from the measurements collected over a long period is presented, as well as a comparison between the real raw data of the BMG160 gyroscope and the designed hardware emulator in both the time and frequency domains. This is done to evaluate the accuracy of the gyroscope model emulating the real sensor in laboratory simulations. The experimental results show that the signals from the emulator and the BMG160 gyroscope are quite close. Therefore, the proposed prototype could be an optimal solution for laboratory calculations and simulations.

Keywords: Allan variance, BMG160 gyroscope, hardware emulator, nanosatellite, power spectral density, stochastic model.

DOI: 10.21303/2461-4262.2023.002528

1. Introduction

A nanosatellite is a type of artificial satellite of small size (usually they are multiples of a 1U cubsat). It's widely used in several military and scientific research applications because of its slightly low cost, and its components have become more accessible than ever [1–3]. From a technical point of view, it allows not only the integration of mechanical components and electric circuits, but also sensors, actuators, microprocessors, and various electrical and optical systems in a very small geometric space. Thus, forming components of compact satellites to carry out a very specific mission [4, 5].

The sensor, in particular the gyroscope, is widely used in almost all nanosatellites and plays an essential role in attitude determination during the whole orbital passage in its life cycle. This electromechanical component contains dynamic oscillating masses that detect the necessary mechanical excitation to convert it into an electrical magnitude [6]. The performance of this equipment is highly dependent on the quality of its sensory performance preset at the factory. However, the gyroscope suffers from several inherent random noises that may not provide accurate results and eventually induce irreversible catastrophic situations if it is not modeled and then compensated [7]. Moreover, the estimation of the measurement noise is a very important step in the modeling

of gyro sensors. Having accurate models close to the real model of the sensor will directly and significantly affect the accuracy of the control chain embedded in the nanosatellite.

In the very near past, the two classical statistical parameters, namely the average and the variance, have been widely used to quantitatively describe the behavior of random noises. Later, the usual statistical laws gradually gave way to other identification and modeling approaches to describe the noise included in the signals. Examples of these approaches contain:

a) power spectral density (PSD) [8];

b) ARMA model technique [9];

c) autocorrelation function [10].

The autocorrelation function approach is not recommended in practice since it requires a very large number of measurements that may be more than the gyroscope's life cycle [11].

In 1966, scientific research discovered that the classical variance diverged with the passing time when analysing the frequency stability of the cesium atomic clock frequency standard. In order to solve this problem, a new evaluation method was proposed, which was later called the Allan variance [12]. Since gyroscopic devices also have the characteristics of oscillators, the Allan variance analysis is also widely used in modeling the random errors of inertial devices. Therefore, the IEEE standard introduces the Allan variance method in the modeling analysis of laser gyroscopes [13]. At the moment, the Allan Variance (AVAR) and Power Spectral Density (PSD) approaches are in great demand for the identification and modeling of stochastic noises, which are defined and detailed in [14]. Currently, there is strong competition in the scientific community to develop efficient methods able to effectively distinguish signal from noises [12, 15].

The noise in the gyroscope signal is typically composed of the following terms:

− quantization noise: When an analog signal is encoded in digital form, one of the faults that can occur is referred to as the bit error rate. It reflects the lowest possible resolution level that the sensor can achieve;

− angle random walk: On gyroscope rate output voltages, this is a high-frequency noise with a white-noise rational spectrum (Gaussian noise);

− bias instability: This noise is caused by electronics or other parts that are subject to random fluctuation. It is also known as flicker noise and is approximated by the first-order Gauss-Markov process;

− rate random walk: It's an unidentified random process, potentially exponentially correlated noise with a prolonged correlation time;

− rate ramp: It is probably due to a very weak acceleration of the platform in the same direction and persisting over a long period of time. As an approximation, the second-order Gauss-Markov process is used. This type of noise is ignored in this work.

The conventional Allan variance plot can be used to identify the above stochastic errors. **Table 1** summarizes the Allan variance coefficients and slopes of the respective curves.

Table 1
Allan variance coefficients and curve slopes

Noise type	Noise coefficient	Curve Slope
Quantization noise	Q	–1
Angle random walk	N	–1/2
Bias instability	B	0
Rate random walk	K	1/2
Rate ramp	R	1

With the continuous expansion of the gyroscope exploitation field in space applications in recent years, the field of hardware emulation of complex systems has gradually expanded. In this perspective, the work presented in this paper proposes the use of a low-cost hardware emulator to practically emulate the BMG160 space gyroscope used in nanosatellites. This emulator allows users to directly and iteratively test and adjust algorithms in a practical virtual simulation

environment before the hardware prototype process begins. This significantly reduces the development budget in terms of cost, time, and risk.

2. Materials and methods

2. 1. Assumptions and simplifications

Frequency and phase instabilities can be characterized by random processes that can be represented statistically either in the Fourier frequency domain or in the time domain. A stochastic model of the studied gyroscope will be detailed in this section. Deterministic uncertainties such as scale factor and misalignment uncertainties are neglected since there is no access to its input and under the assumption that corrections for these uncertainties have been made at the factory. Also, since the studied sensor has a digital resolution of 16 bits, the quantization noise is not taken into account.

2. 2. Allan variance

David W. Allan created the Allan Variance (AVAR) algorithm in 1966 as a simple variance analysis approach, and it was widely used to characterize frequency and phase instability in precision oscillators. AVAR approach is a time domain analysis tool that was originally developed to characterize clock system noise and stability [16].

It is a technique to represent root mean square (RMS) random drift uncertainty as a function of average time, and it can be used to figure out the nature of the random event causing the noise in the data. It is used to describe different types of noise aspects in the gyroscope data by running certain functions on the whole length of the data [12].

AVAR is based on the cluster evaluation method. The data flow is segmented into clusters of varying lengths. N consecutive sample points are given, each with a sampling time τ_0. Each cluster is formed by a collection of n consXVqual to $n\tau_0$ associated with each cluster. If the inertial sensor's instantaneous output rate is $\Omega(t)$, the cluster average is determined as [13]:

$$\bar{\Omega}_k(\tau)=\frac{1}{\tau}\int_{t_k}^{t_k+\tau}\Omega_k(t)\mathrm{d}t, \tag{1}$$

where $\bar{\Omega}_k(\tau)$ represents the cluster average of the output rate for a cluster starting with the k^{th} data point and ending with the $k^{\text{th}}+\tau$ data point (include n data points).

The following cluster mean is defined as follows:

$$\bar{\Omega}_{next}(\tau)=\frac{1}{\tau}\int_{t_k+\tau}^{t_k+2\tau}\Omega_k(t)\mathrm{d}t. \tag{2}$$

From two adjacent clusters, the Alan variance of length τ is calculated as below [14]:

$$\sigma^2(\tau)=\frac{1}{2}\left[\bar{\Omega}_{next}(\tau)-\bar{\Omega}_k(\tau)\right]^2, \text{ or}$$

$$\sigma^2(\tau)=\frac{1}{2(K-1)}\sum_{k=1}^{K-1}\left[\bar{\Omega}_{next}(\tau)-\bar{\Omega}_k(\tau)\right]^2. \tag{3}$$

As with the standard deviation and variance, the Allan deviation is defined as the square root of the Allan variance:

$$\sigma(\tau)=\sqrt{\sigma^2(\tau)}. \tag{4}$$

2. 3. Power spectral density

To describe the instability of oscillators in the frequency domain, let's use spectral density. As a physical interpretation, the power spectral density characterizes the energy distribution of the signal under study in the frequency domain. The main feature that distinguishes the power spectral density (PSD) compared to other spectral analysis approaches is its performance in analysing periodic and non-periodic signals. The (5) shows how the Fourier transform pair, also known as the two-sided PSD, and the autocorrelation function are mathematically related to each other for stationary processes [17]:

$$S(\omega)=\int_{-\infty}^{+\infty}e^{-j\omega\tau}K(\tau)\mathrm{d}\tau, \tag{5}$$

with $S(\omega)$ is the two-sided power spectral density; $K(\tau)$ is the autocorrelation function defined as below:

$$K(\tau)=\int_{-\infty}^{+\infty}\Omega(t+\tau)\Omega^{*}(t)\mathrm{d}t, \text{ or}$$

$$K(\tau)=\int_{-\infty}^{+\infty}\Omega(t)\Omega^{*}(t-\tau)\mathrm{d}t, \tag{6}$$

where * represents the complex conjugate of $\Omega(t)$.

The (7) provides the unique relationship between the AVAR and the PSD [13]:

$$\sigma^{2}(\tau)=4\int_{0}^{\infty}S_{\Omega}(f)\frac{\sin^{4}x}{x^{2}}\mathrm{d}f,\ x=\pi f\tau, \tag{7}$$

where $S_{\Omega}(f)$ denotes the power spectral density of the $\Omega(\tau)$ process, which is considered to be stationary in time.

2. 4. Gyroscope stochastic model

The gyroscope measurement is affected by several types of noise. The three basic noise terms are angle random walk (N), bias instability (B), and rate random walk (K). Assuming that manufacturing uncertainties such as scale factor and misalignment uncertainties are neglected (stationary state $\Omega_{ideal}(t)=0$), the gyroscope output measurement can be modeled by the formula as follow [11, 18, 19].

$$\Omega_{model}(t)=y_{N}(t)+y_{B}(t)+y_{K}(t), \tag{8}$$

where $y_N(t)$ is the uncertainty due to angle random walk; $y_B(t)$ is the uncertainty due to bias instability; $y_K(t)$ is the uncertainty due to rate random walk.

According to (7), the AVAR is proportional to the total noise power of the gyroscope when transmitted through a filter with a transfer function of $\sin^4 x/x^2$. Using this observation, the filter's bandwidth will be set by τ. This means that by adjusting τ or modifying the filter bandwidth, various noise coefficients such as B, N, and K can be found.

The three noise parameters mentioned above, angle random walk (white noise), rate random walk (Brownian noise), and bias instability (flicker noise), are calculated from the recorded data of the stationary gyroscope. They are found by using the relationship between the Allan variance and the one-sided power spectral density (PSD) of the noise parameters in the original data. This relationship is shown in (7). **Table 2** gives the procedure to calculate each noise parameter [20].

Table 2

Procedure used to determine noise parameters using AVAR and PSD

Parameter	Allan value	PSD value
$N\left[^{\circ}/\mathrm{s}/\sqrt{\mathrm{Hz}}\right]$	$\sigma^{2}(\tau)=\frac{N^{2}}{\tau}$	$S_{\Omega}(f)=N^{2}$
$B[^{\circ}/\mathrm{s}]$	$\sigma^{2}(\tau)=\frac{2B^{2}}{\pi}\ln 2$	$S_{\Omega}(f)=\begin{cases}\left(\frac{B^{2}}{2\pi}\right)\frac{1}{f}, & f\le f_{0};\\ 0, & f>f_{0}\end{cases}$
$K\left[^{\circ}/\mathrm{s}/\sqrt{\mathrm{Hz}}\right]$	$\sigma^{2}(\tau)=\frac{K^{2}\tau}{3}$	$S_{\Omega}(f)=\left(\frac{K^{2}}{2\pi}\right)\frac{1}{f^{2}}$

2. 5. Identification of gyroscope noises

A series of long-term data logged from the real gyroscope sensor to Matlab was performed in order to evaluate the noises parameters of the gyroscope embedded in the nanosatellite with a sampling frequency $f_s = 200$ Hz. Statistical average was used to determine the corresponding bias. The actual stationary gyroscope data from the *x*-axis is shown in **Fig. 1**. The output is expected to be zero, but as shown in the figure, the gyroscope output is noisy.

Fig. 2 depicts a histogram representation of the BMG160 sensor's measurements with random noises. The data format demonstrates that the measurements density follows the continuous normal distribution with the following parameters: average $\mu_{gyro} = 0.116359°/s$ and standard deviation $\sigma_{gyro} = 0.249367°/s$. The probability density given by (9) is represented by the red curve:

$$f(x) = \frac{1}{\sigma_{gyro}\sqrt{2\pi}} e^{\frac{-1}{2}\left(\frac{x-\mu_{gyro}}{\sigma_{gyro}}\right)^2}. \quad (9)$$

To determine the different terms of the noise included in the measurements of the gyro, let's study its characteristics in the time and frequency domain. In the time domain, let's use the Allan variance on a log-log scale to precisely determine the parameters *B*, *N*, and *K*. In the frequency domain, let's use the one-sided power spectral density (PSD) of the gyroscopic noise to evaluate the frequency behavior of the noise. The results obtained are shown in **Fig. 3, 4**.

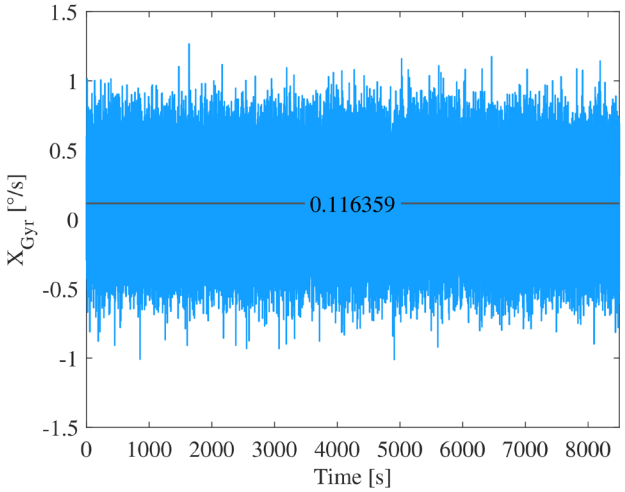

Fig. 1. Raw data of the real gyroscope represented in the time domain

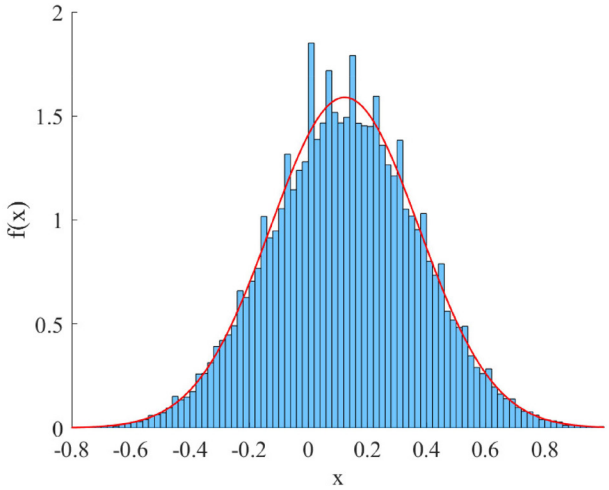

Fig. 2. Representation of measurements in histogram and Gaussian curve

The Allan variance curve, characterizing the measurement noise over a sufficiently long time of the gyroscope *x*-axis, is illustrated in **Fig. 3** on a log-log scale. The abscissa axis represents the grouping time τ of the measurements. It can be decomposed into three zones which are the following:

− the initial descent zone defines the dominance of high-frequency noise. Due to the log-log scale, the Allan variance (deviation) decreases rapidly with a slope of –0.5 which signifies the presence of white Gaussian noise;

− the lowest point of the curve represents the bias instability;

− the rising area indicates the presence of low-frequency noise. This zone is usually due to temperature variation and the sensor life cycle.

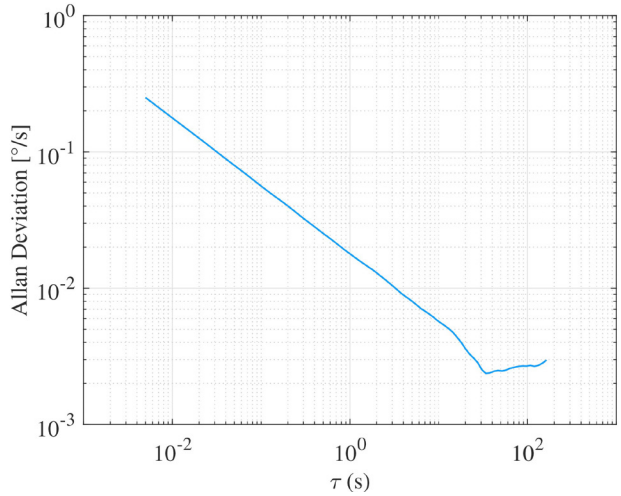

Fig. 3. Allan variance of gyroscope data

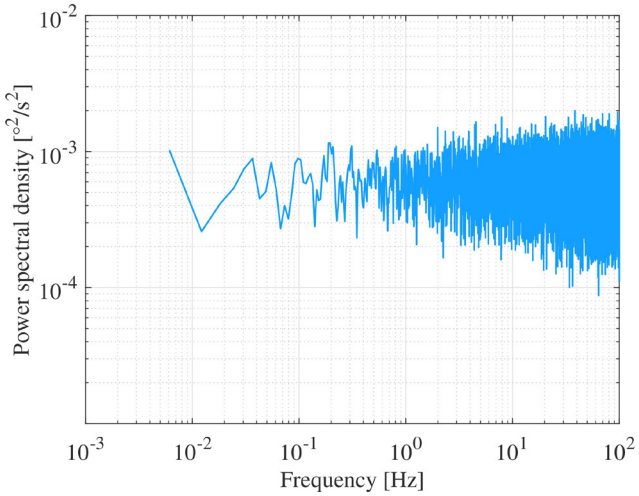

Fig. 4. One-sided power spectral density of gyroscope data

Taking into account the connection between AVAR and the PSD mentioned in (7), as a result: $N = 1.779073 \times 10^{-2}$ °/s/$\sqrt{\text{Hz}}$, $B = 4.047421 \times 10^{-3}$ °/s, and $K = 4.023987 \times 10^{-4}$ °/s/$\sqrt{\text{Hz}}$ are obtained.

2. 6. Hardware emulator modeling

2. 6 1. Bias instability

The differential equation used to describe the bias instability is given as [21]:

$$T\frac{dy_B(t)}{dt} + y_B(t) = \omega(t), \tag{10}$$

where $y_B(t)$ represents a Gauss-Markov process (which is low-frequency noise) and $\omega(t) \sim N(0,1)$ represents white noise. In accordance with **Fig. 3**, let's consider $T = 33.9$ s (lowest point) [21, 22].

Discretizing (10) gives:

$$y_B(k) = \alpha_d y_B(k-1) + b_d \eta(k),\ \eta(k) \sim N\left(0, \sigma_B^2\right), \tag{11}$$

with

$$\alpha_d = e^{-\Delta T/T} = 0.99985253,\ b_d = \int_0^{\Delta T} e^{-t/T} \mathrm{d}t = 0.499963 \times 10^{-2},$$

$$f_s = 200 \text{ Hz, and } \Delta T = \frac{1}{fs} = 5 \times 10^3 \text{ s.}$$

The parameters α_d, b_d, B and σ_B are related by formula (12) below [21, 22].

$$\sigma_B = \frac{B\sqrt{1-\alpha_d^2}}{b_d}. \tag{12}$$

As a result, the numerical calculation gives the following result:

$$\sigma_B = 1.3903 \times 10^{-2}\ ^\circ/\text{s}. \tag{13}$$

Equation (11), therefore, becomes:

$$y_B(k) = \alpha_d y_B(k-1) + b_d \sigma_B \omega_B(k),\ \omega_B(k) \sim N(0,1). \tag{14}$$

2. 6. 2. Rate random walk

The rate random walk is represented by an integrator's reaction to white noise with unknown variance σ_K^2. The discrete-time relationship is provided by [22]:

$$y_K(k) = y_K(k-1) + K\Delta T \sigma_K \omega_K(k),\ \omega_K(k) \sim N(0,1). \tag{15}$$

As illustrated in **Fig. 5**, the value of σ_K is determined by approximating the low-frequency segment of the gyroscopic noise produced by the PSD.

As a consequence, $\sigma_K = 0.102515 \times 10^{-2}\ ^\circ/\text{s}/\sqrt{\text{Hz}}$ is found. The red curve in **Fig. 5** illustrates the random walk rate PSD of the hardware emulator as obtained experimentally.

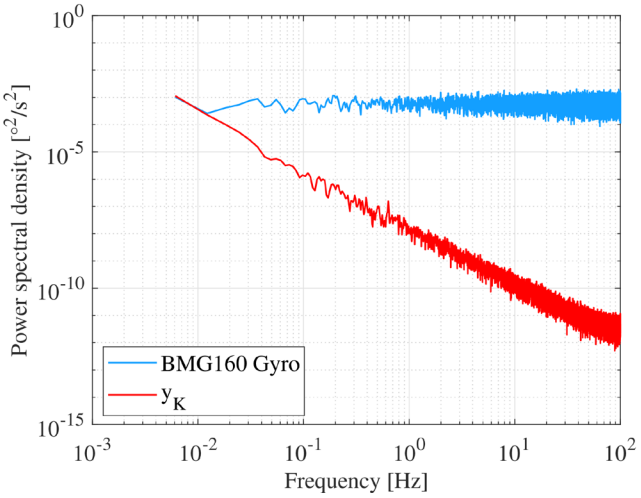

Fig. 5. One-sided random walk approximation of the hardware model

2. 6. 3. Angle random walk

The third type of gyroscope noise relates to the angle random walk (which is high-frequency noise). This noise is represented as a white noise with a variance σ_N calculated by the formula below [22]:

$$\sigma_N = \sqrt{\sigma_{gyro}^2 - B^2 - \left(K\Delta T\sigma_K\right)^2}, \tag{16}$$

(16) gives $\sigma_N = 0.249334\ {}^{\circ}/\mathrm{s}/\sqrt{\mathrm{Hz}}$. So, the model of the angle random walk is given by the expression below:

$$y_N(k) = \sigma_N\omega_N(k),\ \omega_N(k) \sim N(0,1). \tag{17}$$

2. 6. 4. Emulator noise model

After all the noise values have been estimated using the (14), (15), and (17) formulas that were provided already, the noise of the gyroscope can now be written as (18):

$$\Omega_{model}(k) = \sigma_N\omega_N(k) + \alpha_d y_B(k-1) + b_d\sigma_B\omega_B(k) + \\ + y_K(k-1) + K\Delta T\sigma_K\omega_K(k). \tag{18}$$

Where $\omega_N(k)$~$N(0,1)$; $\omega_B(k)$~$N(0,1)$; $\omega_K(k)$~$N(0,1)$.

2. 6. 5. Normal distribution generation

The coefficients σ_N, σ_B, and σ_K mentioned in the previous paragraphs obey the centered reduced normal distribution $N(0,1)$.

To generate these coefficients, the Box-Muller method was used. Box-Muller is an algorithm for generating normally distributed random numbers using uniformly distributed random numbers [23].

If u_1 and u_2 are distributed uniformly and independently in]0,1], then z_1 and z_2 have a normal distribution with mean $\mu_0 = 0$ and variance $\sigma^2 = 1$.

$$z_1 = \sqrt{-2\ln u_1} \times \cos\left(2\pi u_2\right), \tag{19}$$

$$z_2 = \sqrt{-2\ln u_1} \times \sin\left(2\pi u_2\right). \tag{20}$$

2. 7. Electrical diagram

The output of the Bosch BMG160 sensor has the characteristics of Gaussian white noise, Brownian noise, Flicker noise, and low drift, so an accurate hardware model of this gyroscope should be established in order to use it in advanced computational algorithms and simulations laboratory without using a real sensor to reduce the cost of testing and eliminate security risks. The proposed model is detailed in **Fig. 6**.

The proposed model is based on an Atmega 328P-A microcontroller in SMD technology, clocked by an external 16 MHz clock coupled with two capacitors, C1 and C2. When opening the serial port, the RTS goes to state 1, and the capacitor C3 makes it possible to restart the Atmega 328P-A before loading. D1, D2 and D3 are protection components.

The three jumpers JP1, JP2 and JP3 are designed to the selection of the power source:

− JP1: power supply based on an HT7550 regulator;

− JP2: power supply via ICSP connector;

− JP3: power supply via USB/serial converter.

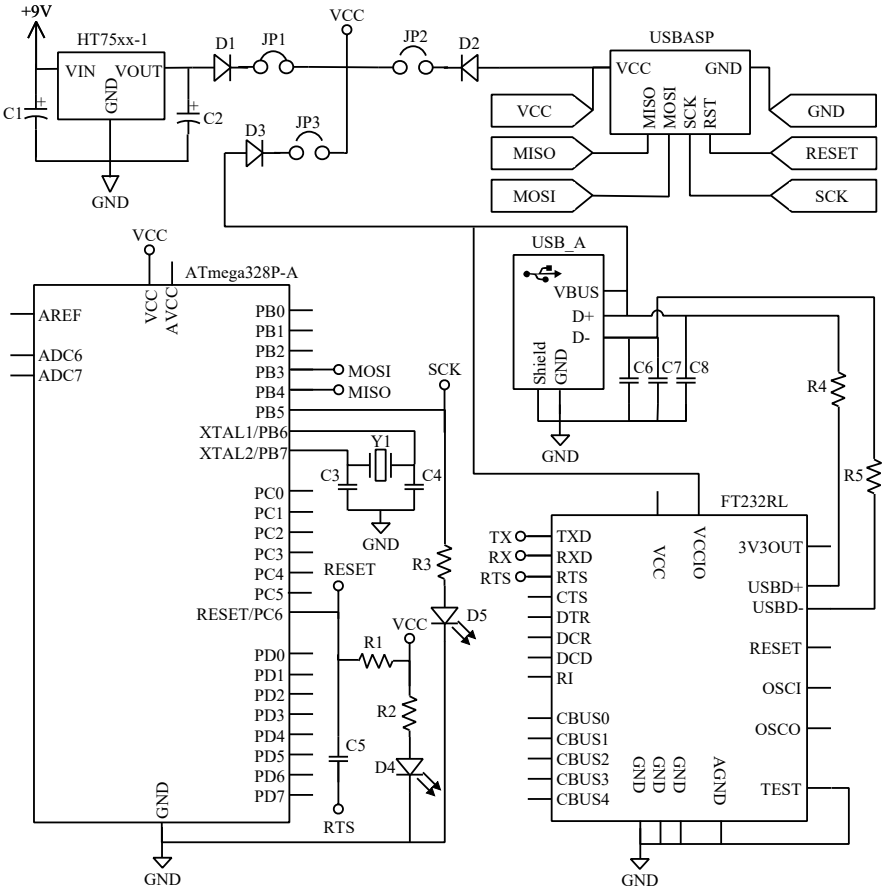

Fig. 6. Proposed hardware emulator for gyroscope BMG160

3. Experimental results and discussions

To evaluate the performance of the model implemented in the microcontroller, a comparison in the time and frequency domains was carried out in order to validate the proposed model. As shown in **Fig. 7**, the proposed emulator's Allan curve matches perfectly with the noise detected along the gyroscope *x*-axis in a stationary state $\left(\Omega_{ideal}(t)=0\right)$. A small shift between the two curves is observed at the tail of the curve. This shift is explained by the quantization, ramp parameters, and effect of temperature, which are not taken into account in the proposed model.

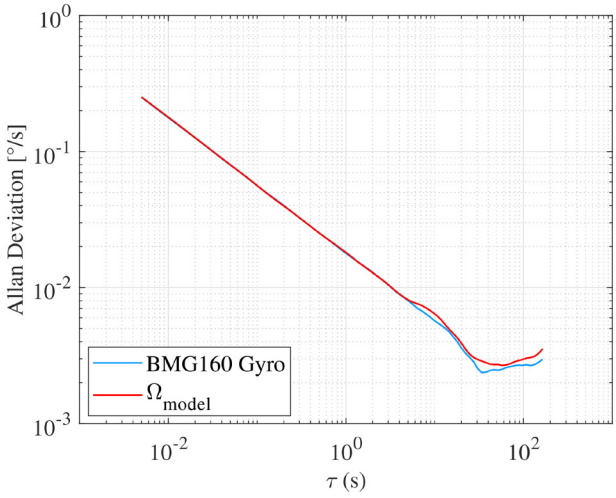

Fig. 7. Allan variance of gyroscope data

The degree of accuracy of the designed gyroscope model is confirmed by comparing its response acquired through the serial port to actual data from the BMG160 gyroscope. The plot of the two responses in frequency domain is shown in **Fig. 8**.

Fig. 9 illustrates a comparison of the raw data collected along the sensor's *x*-axis and gyroscope model data represented in time domain. One can observe the perfect overlapping between the real data and the model data.

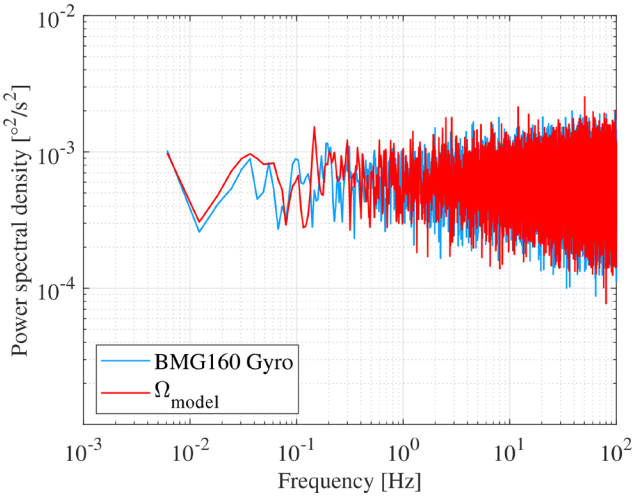

Fig. 8. One-sided frequency spectrum of gyroscope data and model data represented in the frequency domain

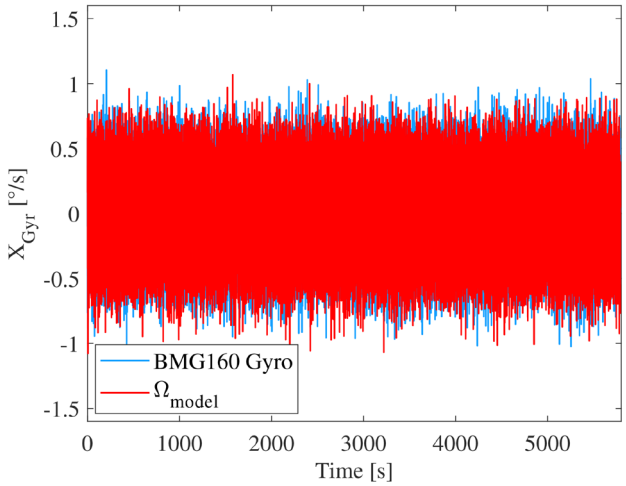

Fig. 9. Collected data from the real and model gyroscopes represented in the time domain

Table 3 is used to compare the accuracy of the designed model after extracting the constant bias of $\mu_{gyro} = 0.116359$°/s. This comparison shows that the signals are quite close. Therefore, it is obvious to affirm that the proposed model is a candidate model for future laboratory calculations and simulations.

Table 3

Comparison between BMG160 gyroscope and gyroscope model

Gyroscope	Average [°/s]	Deviation [°/s]
BMG160	0	0.251087
Model	–0.002635	0.251072

4. Conclusions

This work has allowed to identify the embedded gyroscope in a nanosatellite and to produce an equivalent numerical model to be able to carry out advanced simulations without recourse to the real material to avoid the problem of bad manipulation and material availability. Deterministic uncertainties include scale factors, non-orthogonality, and misalignment of axes, which are assumed to be calibrated by the manufacturer. Stochastic uncertainties contain random uncertainties that cannot be eliminated. For this purpose, the Allan method, based on the calculation of the Allan variance, and power spectral density were introduced to characterize the noise included in measurements collected over a long period. This is a solution that is becoming more and more essential and gives precise estimates independent of the samples size (large sizes), instead of the classic statistical variance, which increases as the measurements increase.

Early phases of nanosatellite hardware development can benefit from this emulator which offers an accuracy of $-2.635e^{-5}$°/s on average and $1.5e^{-5}$°/s in standard deviation. It is useful to carry out advanced tests before the real hardware is present and thus to discover problems and faults. In the same perspective, this hardware emulator will be extended towards the integration of all the components of the control system and the attitude determination of the nanosatellite.

Conflict of interest

The authors declare that there is no conflict of interest in relation to this paper, as well as the published research results, including the financial aspects of conducting the research, obtaining and using its results, as well as any non-financial personal relationships.

Financing

The study was performed without financial support.

Data availability

Manuscript has no associated data.

Acknowledgment

This work was carried out in the frame of the cooperation between the Royal Center for Space Research and Studies (CRERS) and the Mohammed V University in Rabat (UM5R).

References

[1] Pablo, H., Whittaker, G. N., Popowicz, A., Mochnacki, S. M., Kuschnig, R., Grant, C. C. et al. (2016). The BRITE Constellation Nanosatellite Mission: Testing, Commissioning, and Operations. Publications of the Astronomical Society of the Pacific, 128 (970), 125001. doi: https://doi.org/10.1088/1538-3873/128/970/125001

[2] Perez, F., Modenini, D., Vázquez, A., Aguado, F., Tubío, R., Dolgos, G. et al. (2018). DustCube, a nanosatellite mission to binary asteroid 65803 Didymos as part of the ESA AIM mission. Advances in Space Research, 62 (12), 3335–3356. doi: https://doi.org/10.1016/j.asr.2018.06.019

[3] Lucia, B., Denby, B., Manchester, Z., Desai, H., Ruppel, E., Colin, A. (2021). Computational Nanosatellite Constellations. GetMobile: Mobile Computing and Communications, 25 (1), 16–23. doi: https://doi.org/10.1145/3471440.3471446

[4] Kirat, B. (2021). Design of nanosatellite constellations for internet of things applications. Istanbul Technical University. Available at: http://siga.uubf.itu.edu.tr/uubftez/upload/itu/uubf/uzay/Bedirhan_Kirat-uzay-20210614.pdf

[5] Chiu, S.-Y., Kim, K. A., Liu, Y.-C. (2021). Analysis of Nanosatellite Impedance Interaction and Stability Based on System Operation Mode. 2021 IEEE International Future Energy Electronics Conference (IFEEC). doi: https://doi.org/10.1109/ifeec53238.2021.9662020

[6] Du, J., Gerdtman, C., Lindén, M. (2018). Signal Quality Improvement Algorithms for MEMS Gyroscope-Based Human Motion Analysis Systems: A Systematic Review. Sensors, 18 (4), 1123. doi: https://doi.org/10.3390/s18041123

[7] Tanenhaus, M., Geis, T., Carhoun, D., Holland, A. (2010). Accurate real time inertial navigation device by application and processing of arrays of MEMS inertial sensors. IEEE/ION Position, Location and Navigation Symposium. doi: https://doi.org/10.1109/plans.2010.5507137

[8] Lefevre, H. C. (1993). The fiber-optic gyroscope. Artech Print on Demand, 332.

[9] Choi, B. (1992). ARMA Model Identification. Springer New York, 200. doi: https://doi.org/10.1007/978-1-4613-9745-8

[10] Ding, M., Shi, Z., Du, B., Wang, H., Han, L. (2021). A signal de-noising method for a MEMS gyroscope based on improved VMD-WTD. Measurement Science and Technology, 32 (9), 095112. doi: https://doi.org/10.1088/1361-6501/abfe33

[11] Saini, V., Rana, S., Kube, M. (2010). Online estimation of state space error model for MEMS IMU. Journal of Modelling & Simulation of Systems, 1 (4), 219–225.

[12] Allan, D. W. (1987). Time and Frequency (Time-Domain) Characterization, Estimation, and Prediction of Precision Clocks and Oscillators. IEEE Transactions on Ultrasonics, Ferroelectrics and Frequency Control, 34 (6), 647–654. doi: https://doi.org/10.1109/t-uffc.1987.26997

[13] El-Sheimy, N., Hou, H., Niu, X. (2008). Analysis and Modeling of Inertial Sensors Using Allan Variance. IEEE Transactions on Instrumentation and Measurement, 57 (1), 140–149. doi: https://doi.org/10.1109/tim.2007.908635

[14] Tehrani, M. M. (1983). Ring Laser Gyro Data Analysis With Cluster Sampling Technique. SPIE Proceedings. doi: https://doi.org/10.1117/12.935818

[15] Han, S., Meng, Z., Zhang, X., Yan, Y. (2021). Hybrid Deep Recurrent Neural Networks for Noise Reduction of MEMS-IMU with Static and Dynamic Conditions. Micromachines, 12 (2), 214. doi: https://doi.org/10.3390/mi12020214

[16] Allan, D. W. (1966). Statistics of atomic frequency standards. Proceedings of the IEEE, 54 (2), 221–230. doi: https://doi.org/10.1109/proc.1966.4634

[17] Curey, R. K., Ash, M. E., Thielman, L. O., Barker, C. H. (2004). Proposed IEEE inertial systems terminology standard and other inertial sensor standards. PLANS 2004. Position Location and Navigation Symposium (IEEE Cat. No.04CH37556). doi: https://doi.org/10.1109/plans.2004.1308978

[18] Fossen, T. I. (2011). Handbook of Marine Craft Hydrodynamics and Motion Control. John Wiley & Sons, Inc. doi: https://doi.org/10.1002/9781119994138

[19] El Fatimi, A., Addaim, A., Guennoun, Z. (2021). A low-cost IMU/GPS position accuracy experimental study using extended kalman filter data fusion in real environments. E3S Web of Conferences, 297, 01040. doi: https://doi.org/10.1051/e3sconf/202129701040

[20] 952-1997. IEEE Standard Specification Format Guide and Test Procedure for Single-Axis Interferometric Fiber Optic Gyros. doi: https://doi.org/10.1109/ieeestd.1998.86153

[21] Langel, S., Crespillo, O. G., Joerger, M. (2019). Bounding Sequential Estimation Errors Due to Gauss-Markov Noise with Uncertain Parameters. ION GNSS+, The International Technical Meeting of the Satellite Division of The Institute of Navigation. doi: https://doi.org/10.33012/2019.17014

[22] Petkov, P., Slavov, T. (2010). Stochastic modeling of MEMS inertial sensors. Cybernetics and information technologies, 10 (2), 31–40. Available at: https://cit.iict.bas.bg/CIT_2010/v10-2/31-40.pdf

[23] Addaim, A., Gretete, D., Madi, A. A. (2018). Enhanced Box-Muller method for high quality Gaussian random number generation. International Journal of Computing Science and Mathematics, 9 (3), 287. doi: https://doi.org/10.1504/ijcsm.2018.093153

Received date 10.08.2022
Accepted date 16.12.2022
Published date 19.01.2023

How to cite: *El Fatimi, A., Addaim, A., Guennoun, Z. (2023). Development of a hardware emulator of a nanosatellite gyroscope. EUREKA: Physics and Engineering, 1, 42–53. doi: https://doi.org/10.21303/2461-4262.2023.002528*